Surface plasmon excitation on a single subwavelength hole in a metallic sheet

Evgeny Popov, Nicolas Bonod, Michel Nevière, Hervé Rigneault, Pierre-François Lenne, and Patrick Chaumet

The diffraction of light by a single subwavelength hole in a highly conductive metallic sheet is analyzed with a recently developed differential theory that is able to plot the nearly electromagnetic field. Using rigorous electromagnetic and phenomenological analysis, we show that a single subwavelength hole can excite surface-plasmon resonance that contributes greatly to extraordinary transmission.

OCIS codes: 050.1220, 050.1940, 240.6680.

1. Introduction

Extraordinary transmission[1] by subwavelength-hole arrays has attracted a great amount of interest in the past 6 years and offers promising applications in physics and biology.[2] Recently it was shown that a single subwavelength hole surrounded by circular corrugation exhibits similar extraordinary transmission.[3,4] In such structures the diffraction phenomenon cannot be analyzed in the context of classical optics, even for a single circular hole, and requires a full electromagnetic analysis. As a result, polarization effects, as well as electromagnetic resonances, are found. Among them, surface-plasmon resonances are especially important, as they are suspected to play a key role in enhancing the transmission of light.[5] It is thus interesting to develop a deep understanding of the process, despite the great amount of research that was already done to study transmission by hole arrays. Only a few electromagnetic theories exist with which to analyze diffraction by devices described in cylindrical coordinates. The modal method[6] was recently adapted to analyze coaxial aperture arrays but is unable to analyze isolated holes. Recently the finite-difference time-domain method was applied with success to analyzing subwavelength elliptical holes[7] thanks to a local grid refinement. We followed a completely different way to analyze holes that takes advantage of a recent breakthrough[8] in grating theory and termed fast Fourier factorization.[9,10] The result is a generalization of the differential theory to diffraction by devices described in cylindrical coordinates.[11] In such a geometry the electromagnetic field is represented on a Fourier–Bessel basis, which has to be truncated for numerical computation. After having developed new factorization rules[8,12] with which to derive the component of a product of two functions from the components of each function, i.e., rules that are valid on an arbitrary continuous function basis, we obtained a formulation of Maxwell equations on a truncated Fourier–Bessel basis that yields numerical results that rapidly converge when the truncation order is increased. We applied this theory, named fast numerical factorization, here to investigate in detail the diffraction of light by a single circular hole in a plane metallic sheet. We observed strong asymmetry (namely, lack of cylindrical symmetry) in the electromagnetic field distribution that is caused by the linear polarization of the incident light. At the edges of the hole, where the incident electric field vector is perpendicular to the metal–air borders, there are regions with a sharp increase of electric field amplitude, usually known as the edge effect. The effect is due to charge accumulation caused by the discontinuity of the induced electric current.[7] The charges have opposite signs at opposite edges of the hole, thus forming an electric dipole.[7] This electric field enhancement excites a surface-plasmonlike wave that propagates (with an exponentially decreasing amplitude) along the surface away from the hole, as was demonstrated in the

The authors are with the Institut Fresnel, Case 161, Unité Mixte de Recherche 6133, Faculté des Sciences et Techniques de St-Jérôme, 13397 Marseille Cedex 20, France. E. Popov's e-mail address is e.popov@fresnel.fr.

Received 2 September 2004; revised manuscript received 17 November 2004; accepted 18 November 2004.

0003-6935/05/122332-06$15.00/0

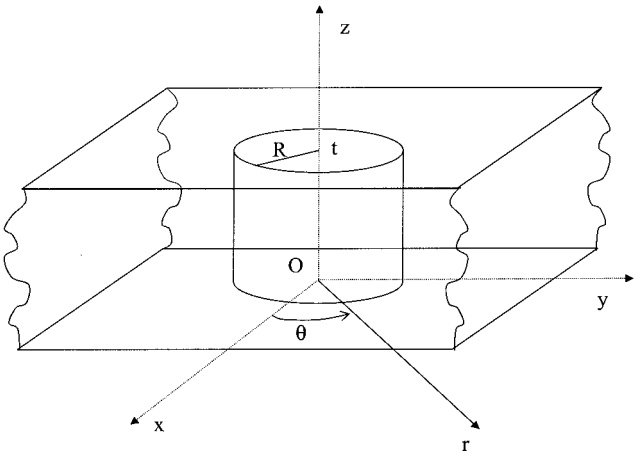

Fig. 1. Schematic representation of a hole in a metallic sheet.

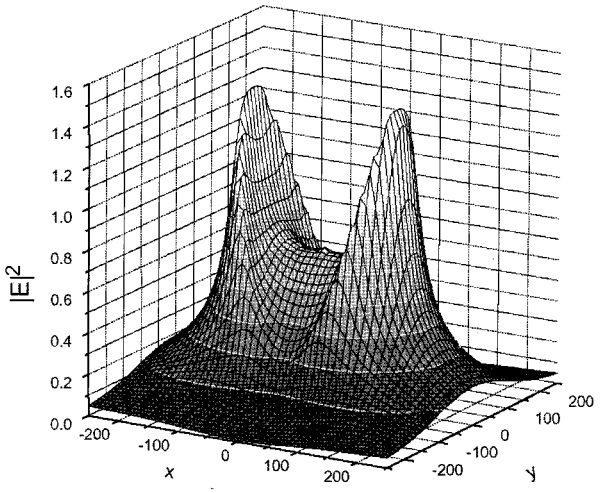

Fig. 2. Map of the square modulus of the electric field obtained at $z = -15$ nm (distances are in nanometers).

research reported in Ref. 13. In addition to this plasmon field, we can distinguish another contribution to the field, which declines as $1/\rho$, where ρ is the distance between the observation point and the hole edge, a contribution that represents a field radiated by the dipole.

2. Description of the Device

The device under study is shown in Fig. 1. It consists of a cylindrical hole with a circular cross section with radius $R = 0.125$ μm that has been made in a plane metallic sheet of thickness $t = 0.2$ μm. The axis of the cylinder is Oz, and xOy is the plane bottom interface of the sheet. All media are isotropic and homogeneous; the superstrate, the substrate, and the hole are in vacuum. The sheet is made from a highly conducting metal with complex refractive index $n = 0.52 + i2.88$. This value is close to the refractive index of silver, but to prevent convergence problems caused by the metal's very high conductivity,[11] we increased the real part of the index tenfold. A monochromatic plane wave falls upon the sheet under normal incidence, with a unit amplitude vector $\mathbf{E}$ parallel to the x axis. The wavelength in vacuum is 0.5 μm. Our aim is to study the field characteristics in the vicinity of the hole and to demonstrate surface-plasmon excitation. The wavelength-to-radius ratio is chosen in such a way that a fundamental mode that could propagate in a hollow cylindrical waveguide with the same radius is below the cutoff.

3. Field Maps Near the Hole

Resolving the boundary-value problem with the fast numerical factorization described in Refs. 9–11 allows any field component to be determined in any region near or inside the hole. Figure 2 shows square modulus $|E|^2$ of the total electric field as a function of x and y coordinates for $z = -15$ nm, i.e., slightly below the lower interface of the sheet. It clearly appears that, despite the cylindrical symmetry of the hole, the field map is not cylindrically symmetric; a privileged direction, namely, the x axis, is determined by the polarization of the incident field. Along the y direction, $|E|^2$ as a function of x exhibits two sharp peaks approximately twice higher than its value at the center ($x = y = 0$), separated by a distance close to 0.25 μm, i.e., by the hole diameter. The sharp peaks appear in the area where the electric field is almost perpendicular to the metal boundary. The boundary conditions thus predict strong charge density. $|E|^2$ is much lower in the regions where $\mathbf{E}$ is tangential to the surface, however, as was already demonstrated in Ref. 7. Similar field maps were recently measured experimentally by other authors.[5]

Figure 3 shows a map of the modulus of the z component of the total electric field under the same conditions as for Fig. 2 ($z = -15$ nm). Although the z component of the incident electric field is zero, two peaks appear for the z component of the total field along the y axis, situated in the vicinity of the hole edges. The curve in Fig. 4, which shows $|E_z|$ as a function of x, points out the existence of extremely sharp peaks as well as of thin fluctuations that are

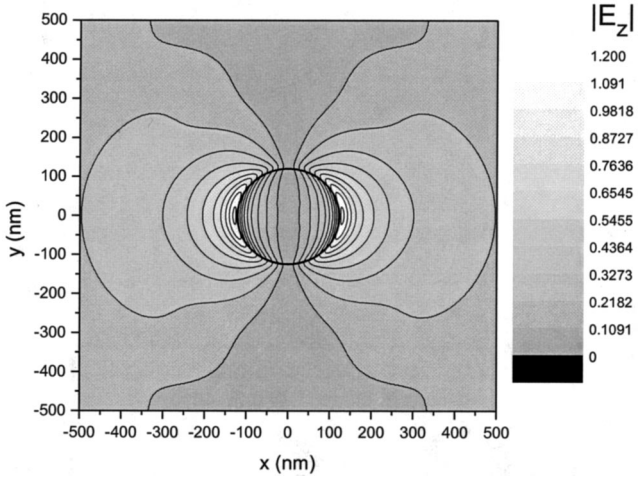

Fig. 3. Map of $|E_z|$ at $z = -15$ nm; the location of the hole's cross section is represented by a thick circle.

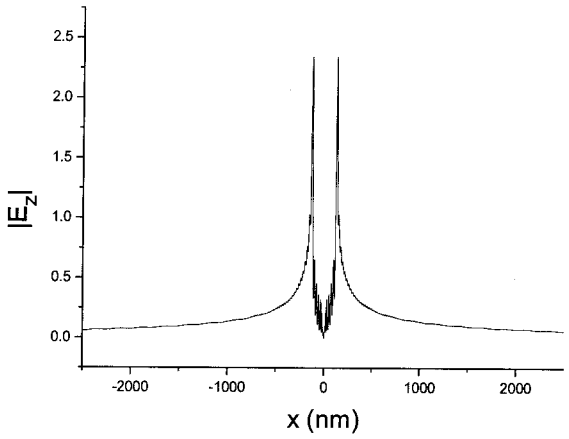

Fig. 4. Variation of $|E_z|$ for $y = 0$ and $z = -1$ nm as a function of x.

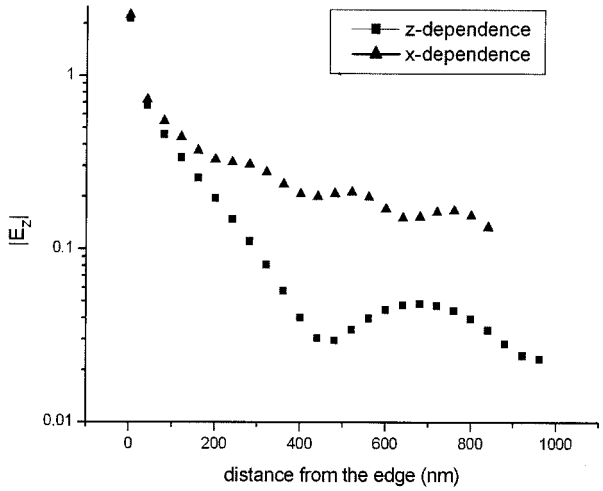

Fig. 6. Variation of $|E_z|$ in the xOz plane below the hole: triangles, $|E_z|$ as a function of x at $z = 0$; squares, $|E_z|$ as a function of z along the line $x = R$ that crosses the hole ridge.

due to the Gibbs phenomenon that results from the reconstruction of a function that has sharp variations at $z = 0$ (metal surface) from its truncated Fourier–Bessel representation. As one can see, $|E_z|$ is equal to zero at $x = 0$, as can be expected from symmetry considerations. To get a better insight into the field topography, we show in Fig. 5 an $|E_z|$ field map in the xOz plane. The location of the hole edge is shown by an arrow. From the shape of equal-amplitude field lines, it is evident that the decrease of $|E_z|$ is much slower in the x direction (i.e., along the metallic surface) than in the z direction (going away from the surface). This is better shown in Fig. 6, which represents two cuts made in Fig. 5, one along the line $z = 0$, which shows the x dependence of $|E_z|$, and the other along the line $x = R$, showing the z dependence. Keeping in mind the logarithmic scale in ordinate, we note that the z decrease is much faster because no surface wave can contribute to propagation of the field in that direction.

The other two electric field components demonstrate similar tendencies. Figure 7 shows the behavior of $|E_r|$, which is close to unity for $x = 0$ and decreases sharply for $x > 0.125$ μm, i.e., outside the hole; the thin fluctuations still occur from the Gibbs phenomenon. Figure 8 shows a smooth curve, however, as it represents $|E_\theta|$ as a function of y instead of x. The incident electric field vector is tangential to the hole boundaries (at $y = \pm 0.125$ μm), so no charge accumulation is observed. This curve culminates in a value close to the incident field's amplitude and tends to zero when $|y|$ is increased, as can be observed in the field map in Fig. 3. We may remark that anyway two small fluctuations occur when $y = \pm R$ that are due to the discontinuity of the normal derivative of $|E_\theta|$ at the hole boundaries.

To determine the field behavior in detail, and, in particular, to demonstrate the plasmon excitation on the metallic surface in the x direction, it is easier to work first in Fourier–Bessel space rather than in coordinate space. This analysis is favored by the fact our method works with the field components in Fourier–Bessel space.

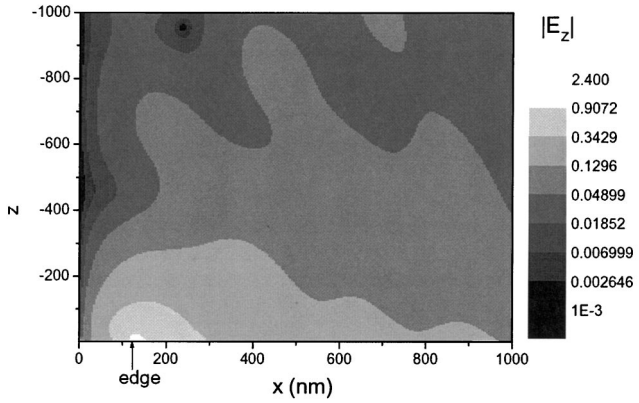

Fig. 5. $|E_z|$ field map of the xOz plane below the hole. For reasons of symmetry, only positive values of x are considered.

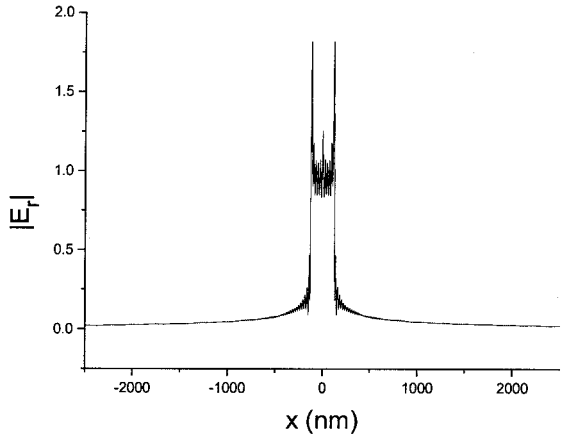

Fig. 7. Same as in Fig. 4 but for $|E_r|$.

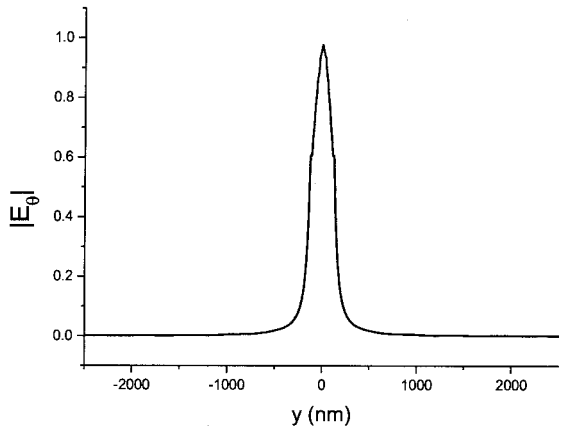

Fig. 8. Variation of $|E_\theta|$ for $x = 0$ and $z = -1$ nm as a function of y.

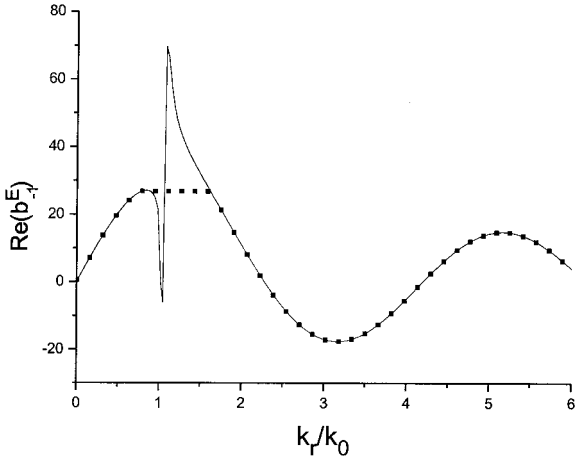

Fig. 9. $\mathrm{Re}(b^E_{-1})$ as a function of the normalized radial wave-vector component.

4. Fourier–Bessel analysis

On a truncated Fourier–Bessel basis, the field components are represented as discrete and finite sums of Bessel functions of integer orders $(n + 1)$ and $(n - 1)$ (Ref. 14):

$$E_r(r, \theta, z) = i \sum_{n=-N}^{N} \sum_{m=0}^{\mathrm{Max}} \Delta k_m [b^E_{n,m}(z) J_{n+1}(k_m r) - c^E_{n,m}(z) J_{n-1}(k_m r)] \exp(in\theta),$$

$$E_\theta(r, \theta, z) = \sum_{n=-N}^{N} \sum_{m=0}^{\mathrm{Max}} \Delta k_m [b^E_{n,m}(z) J_{n+1}(k_m r) + c^E_{n,m}(z) J_{n-1}(k_m r)] \exp(in\theta), \quad (1)$$

where k_m are the discretized values of k_r, the r component of the wave vector of each spectral component of the field. Similar expansions are valid for the magnetic field, with amplitudes denoted by superscript H. For a normally incident plane wave, its only nonzero k_m components are those with k_0. For a perfect metallic sheet without a hole the reflected and transmitted fields contain wave-vector components that reduce to k_0 only. When a surface perturbation (hole, bump, etc.) is introduced, however, the diffracted field contains all the components with k_m that are equal to or different from zero, including evanescent waves.

For a normally incident plane wave it can be shown theoretically that the most important contribution to the sum in Eq. (1) is given by the amplitudes $b^E_{\pm 1,m}$ and $c^E_{\pm 1,m}$. Their behavior as functions of m is quite similar, and the thin curve in Fig. 9 shows the real part of one of the Fourier–Bessel (i.e., spectral) field amplitudes b^E_{-1} as a function of the discretized values k_m of radial wave number k_r, normalized to wave number k_0 of the incident wave in the superstrate. At normal incidence, k_0 is equal to the 0th diffraction order k_0 of the incident field. As can be expected, the existence of the hole generates all the k_m components in the diffracted field. Components with $k_r/k_0 > 1$ correspond to waves that are evanescent in the z direction.

A sharp variation (anomaly) is observed for values of k_r/k_0 slightly higher than 1. This curve resembles the Lorentzian-shaped anomalies that are due to guided-wave excitation in diffraction grating efficiency curves.[15]

A plasmon surface wave propagating along a plane metal–dielectric interface has a propagation constant α that can easily be determined from the refractive indices of the metal and the dielectric.[15] In our case its normalized value is equal to $\tilde{\alpha} = \alpha/k_M = 1.05892 + i0.02431$. The coupling of the plasmon waves propagating along the two boundaries of the metallic layer slightly changes this value, but with the chosen thickness of the layer, $t = 0.2$ μm, the change is almost negligible, as we verified with independent numerical methods. As can be observed from Fig. 9, the position of the peak of the anomaly coincides with the real part of the normalized propagation constant of the unperturbed plasmon, which is a good indication of their common nature. To further convince ourselves of this and to separate the different contributions quantitatively, we made a numerical experiment by artificially suppressing the anomaly in the spectral behavior of b^E_{-1}, c^E_{+1}, b^H_{-1}, and c^H_{+1}, as shown for b^E_{-1} by the filled squares in Fig. 9. This artificial distribution of the reconstructed spatial variation of $|E_z|$ is further called $|E_{z,\,\mathrm{no\ plasmon}}|$ and is shown in Fig. 10(b) in which it is compared to the true values of E_z given by the thin solid curve in Fig. 10(a). It is important to notice the change in the ordinate scale and thus an important reduction of the values of $|E_z|$. Moreover, its x dependence is quite different. Despite the strong oscillations, one can determine the rate of decrease, shown as a thicker curve in Fig. 10(b) and drawn as a function proportional to $1/\rho$, where $\rho = |x - R|$ is the distance from the hole edge:

$$|E_{z,\,\mathrm{no\ plasmon}}| = \frac{C_{\mathrm{no\ plasmon}}}{|x - R|}. \quad (2)$$

Numerical fitting gives the value for $C_{\mathrm{no\ plasmon}} \approx 21$.

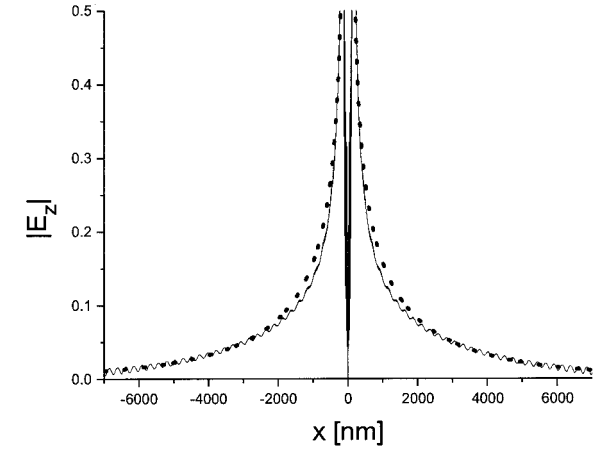

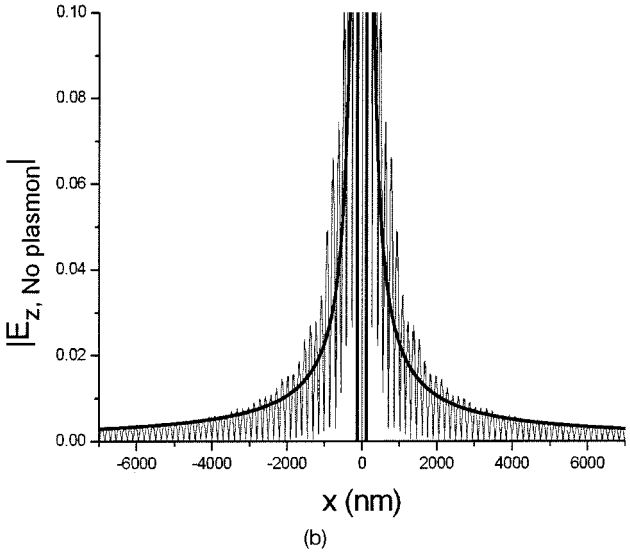

Fig. 10. (a) Thin, solid curve, the same as in Fig. 4 but on a different scale; thick dotted curve, fitting by the sum of Eq. (2) and expression (3). (b) Thinner curve, dependence of $|E_{z,\text{no plasmon}}|$ as a function of x for $y = 0$ and $z = -1$; thicker curve, fit by Eq. (2).

An additional argument for expecting the existence of this contribution comes from Fig. 9, in which the behavior of spectral component b^E_{-1} looks like that of a sinusoid when k_r/k_0 is further increased, with a period in the k_r space close to $2\pi/R$. The integral of the product of the basic function $J_0(k_r, r)$ and the function $\sin(k_r R)$ can be evaluated analytically and outside the interval $x \in [-R, R]$ is proportional to $1/\rho$. Thus the conclusion from the analysis in both real space and k_r space is that the no-plasmon contribution is the field radiated by the electric dipole (at least, relatively far from the source).

Let us go now to the remaining part of the field, to see whether it is really a plasmon contribution. The difference between the values of $|E_z|$ [Fig. 4 or Fig. 10(a)] and $|E_{z,\text{ no plasmon}}|$ [Fig. 10(b)] is plotted in Fig. 11 by a thin, wavy curve. The logarithmic vertical scale enables us to find the exponential decay when we are going away from the hole. More precisely, the fit (thicker curve) is better made with the function

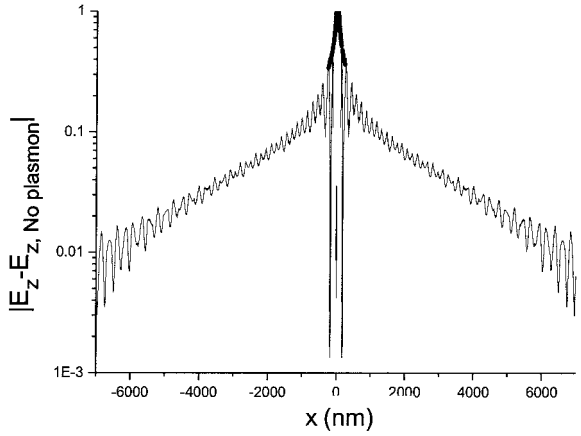

Fig. 11. Thin, wavy curve, the same as in Fig. 10 but for $|E_{z,\text{plasmon}}|$; thicker curve fit by expression (3).

$$\frac{C_{\text{plasmon}}}{\sqrt{x}}\exp(i\alpha'' x), \tag{3}$$

where α'' is the imaginary part of the plasmon propagation constant on the plane metal–air interface and numerical fitting gives the value for $C_{\text{plasmon}} \approx 6$. The factor in the denominator of expression (3) can be explained by the fact that the propagation of the plasmon is made not only in the x direction but along the entire surface. During the preparation of this paper, we found a paper[13] that confirms this behavior but does not take into consideration the nonplasmonic scattering given by Eq. (2). More precisely, Fig. 10(a) exhibits the same x dependence of $|E_z|$ as in Fig. 4 (the thin solid curve) but on a wider x scale, together with the sum of the two contributions, Eq. (2) and expression (3) (thick dotted curve). As can be observed, the decrease of the field combines two effects: first, plasmon propagation (exponential decay plus cylindrical expansion on the surface), with the plasmon excited at the ridge of the hole in the direction perpendicular to the incident field polarization, and second, a spherical decrease of the radiated wave that originated at the charge accumulation points.

Similar curves were obtained for the E_r component of the field, which are not considered here. One can trace the same two contributions, given by Eq. (2) and expression (3), with the same ratio between the fitting constants $C_{\text{no plasmon}}/C_{\text{plasmon}}$ as for $|E_z|$. On the contrary, no plasmon contribution can be found in component E_θ of the field that is tangential to the hole edge.

5. Conclusions

Using rigorous electromagnetic analysis, we studied the transmission of light through a subwavelength hole. An electric field map of the area below the hole and in its vicinity has shown that there are two main contributions to the transmitted field: plasmon excitation produced by the ridges of the hole, which are almost normal to the electric vector of the incident

field, and much weaker (in the case studied) radiation from the electric dipole formed by the charge accumulated at the same points. Thus the role of surface-plasmon excitation in the extraordinary transmission of light is clearly established.

References

1. T. W. Ebbesen, H. J. Lezec, H. F. Ghaemi, T. Thio, and P. A. Wolff, "Extraordinary optical transmission through subwavelength hole arrays," Nature **391,** 667–669 (1998).
2. M. J. Levene, J. Korlach, S. W. Turner, M. Foquet, H. G. Craighead, and W. W. Webb, "Zero-mode waveguides for single-molecule analysis at high concentrations," Science **299,** 682–686 (2003).
3. F. J. Garcia-Vidal, L. Martin-Moreno, H. J. Lezec, and T. W. Ebbesen, "Focusing light with a single subwavelength aperture flanked by surface corrugations," Appl. Phys. Lett. **83,** 4500–4502 (2003).
4. L. Martin-Moreno, F. J. Garcia-Vidal, H. J. Lezec, A. Degiron, and T. W. Ebbesen, "Theory of highly directional emission from a single subwavelength aperture surrounded by surface corrugations," Phys. Rev. Lett. **90,** 167401 (2003).
5. A. Degiron, H. Lezec, N. Yamamoto, and T. Ebbesen, "Optical transmission properties of a single subwavelength aperture in a real metal," Opt. Commun. **239,** 61–66 (2004).
6. A. Moreau, G. Granet, F. I. Baida, and D. Van Labeke, "Light transmission by subwavelength square coaxial aperture arrays in metallic films," Opt. Express **11,** 1131–1136 (2003), http://www.opticsexpress.org.
7. R. Zakharian, M. Mansuripur, and J. V. Moloney, "Transmission of ligth through small elliptical apertures," Opt. Express **12,** 2631–2648 (2004), http://www.opticsexpress.org.
8. L. Li, "Use of Fourier series in the analysis of discontinuous periodic structures," J. Opt. Soc. Am. A **13,** 1870–1876 (1996).
9. E. Popov and M. Nevière, "Maxwell equations in Fourier space: fast converging formulation for diffraction by arbitrary shaped, periodic, anisotropic media," J. Opt. Soc. Am. A **18,** 2886–2894 (2001).
10. M. Nevière and E. Popov, *Light Propagation in Periodic Media: Differential Theory and Design* (Marcel Dekker, New York, 2003).
11. N. Bonod, E. Popov, and M. Nevière, "Differential theory of diffraction by finite cylindrical objects," J. Opt. Soc. Am. A (to be published).
12. E. Popov, M. Nevière, and N. Bonod, "Factorization of products of discontinuous functions applied to Fourier–Bessel basis," J. Opt. Soc. Am. A **21,** 46–52 (2004).
13. L. Yin, V. K. Vlasko-Vlasov, A. Rydh, J. Pearson, U. Welp, S. H. Chang, S. K. Gray, G. C. Schatz, D. B. Brown, and C. W. Kimball, "Surface plasmons at single nanoholes in Au films," Appl. Phys. Lett. **85,** 467–469 (2004).
14. A. Snyder and J. Love, *Optical Waveguide Theory* (Chapman & Hall, London, 1983).
15. R. Petit, ed., *Electromagnetic Theory of Gratings* (Springer-Verlag, Berlin, 1980), Chap. 5.